Characterization and Modeling of the Impedance between Dipole and Loop – Cocentered but Nonorthogonally Oriented

Gerald P. Arada, *Member, IAENG*

***Abstract*—Cocentered Orthogonal Loop and Dipole (COLD) antenna has been effectively used for polarization estimation and direction finding. One important feature of the COLD is the nonpresence of electromagnetic mutual coupling due to the orthogonality between the loop plane and dipole axis. This orthogonality may not be maintained in practical situations. For a dipole and a loop - cocentered but with their axes skewed (a.k.a. slanted, i.e., not perpendicular) - this paper proposes a simple closed form of their electromagnetic mutual impedance and self-impedances, in terms of the two antennas skew angle, the dipole length, and the loop circumference. Using "EMCoS Antenna VLab", the mutual impedance between the dipole and loop and their self-impedances were determined. The best fit model of the real-valued scalars, namely, the magnitude of the mutual impedance and magnitude and phase of self-impedances are selected according to the goodness-of-fit R^2 or "coefficient of determination" and the number of optimized coefficients in the candidate models. The best fit models are then related to pertinent electromagnetic principles.**

***Index Terms*—COLD antenna, dipole and loop antenna array, method of moments, mutual coupling, mutual impedance, modeling of mutual impedance.**

I. Introduction

Composite antenna is preferred over single antenna for favorable radiation characteristics and improved overall communication performance [1]. Loop-dipole composite antenna [2], [3], [4] increases directivity gain over a single loop or a single dipole antenna. The loop-dipole composite antennas are widely used in broadband or multiband wireless applications. A study in [5] designed a compact and unidirectional loop-dipole composite for medical diagnostic and wideband microwave-based applications, while [6] proposed a planar wideband composite antenna composed of an antipodal loop radiator and a symmetrical dipole.

A very popular configuration of a loop-dipole composite antenna is the Cocentered Orthogonal Loop and Dipole (COLD) antenna pair. The orthogonality between the dipole axis and loop plane, if maintained, ensures that the magnetic loop and electric dipole moment are aligned. Hence, on any plane orthogonal to the dipole axis, the omnidirectional characteristic of the COLD antenna pair is maintained.

[7] used the COLD antenna to a borehole radar in order to obtain additional information on the polarization state of the arrival waves. The COLD antenna pair's use in the polarizarization and/or arrival-angles estimations are investigated in [8], [9], [10], [11], [12], [13], [14], [15], [16], [17], [18], [19], [20], [21], [22], [23].

COLD antenna has also been popularly used as an element of a uniform linear [24], [25] and non-uniform linear arrays [26], [27] for a more efficient range, polarization and direction-of-arrival estimations. The uniform linear array consisting of COLD antenna pair elements presents polarization sensitive properties suitable for the source localization of narrowband far-field and time-varying sources, direction finding, and near-field and far-field source signals beamforming.

Computer electromagnetics (CEM) simulation packages, such as Method of Moments (MoM)-based antenna simulation software, have been very useful in characterizing and modeling the electromagnetic fields interaction in antenna arrays. Veering away from the use of analytical methods which often involves complicated integration and nested summations, these antenna simulation software provide quicker computations without sacrificing the accuracy of the results. [38], [39], [40], [41] are some of the works that implemented MoM-based computer simulation tools on their research. [42] investigated the electromagnetic mutual coupling between two orthogonal loops by changing the location of the loop's feedpoint. Using the "EMCoS Antenna VLab", the authors were able to generate numerical values and show clearer 3D illustrations of the mutual and self-impedances of the orthogonal loops. [43] modeled the mutual coupling between skewed crossed dipoles by varying the dipoles' length, separation and skew angle using the "EMCoS Antenna VLab" in computing the mutual impedance.

Indeed, the COLD antenna pair has been physically implemented in [44], [45]. The COLD antenna pair's various electromagnetic characteristics (e.g., bandwidth, polarization, quality factor, radiation pattern, self-impedance) have been analyzed in [46], [47], [48].

Indeed, if the dipole axis and the loop plane are perfectly perpendicular, no mutual coupling would exist. However, this ideality may be unrealized in practical situations.

This work will characterize and model the mutual impedance and self-impedances resulting from a nonorthogonality between the loop and the dipole and will investigate how the mutual impedance and self-impedances would be affected by the dipole length, the loop circumference, the skew angle, and the rotational angle.

Manuscript received October 20, 2021; revised June 11, 2022. This work is supported by the University Research Coordination Office (URCO) under the Vice Chancellor for Research and Innovation (VCRI) of De La Salle University, Manila, Philippines, through the Research Grant for New Ph.D. Program with Project Number 05 N 1TAY18-2TAY20.

G. P. Arada is an Associate Professor of the Department of Electronics and Computer Engineering, De La Salle University, Manila, Philippines. (phone: +639178242027; e-mail: gerald.arada@dlsu.edu.ph)

II. A Skewed COLD Antenna Pair

Fig. 1 shows a cocentered and skewed pair of an extremely thin circular loop of radius R lying on the x-y plane and an infinitesimally thin center-fed dipole of length L. The dipole is skewed by a polar angle φ from the z-axis and rotated from the loop's feeding gap by an azimuth angle β.

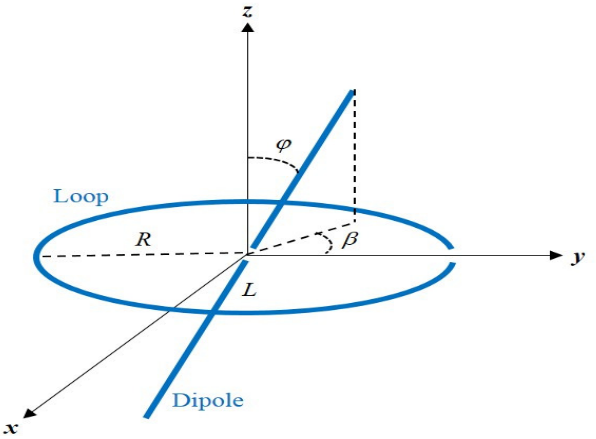

Fig. 1. The geometry of a cocentered nonorthogonal loop and dipole antenna pair .

III. Mutual Coupling and Mutual Impedance

In this paper, the electromagnetic mutual coupling between the loop and dipole antenna pair in Fig. 1 will be exhibited by their mutual impedance.

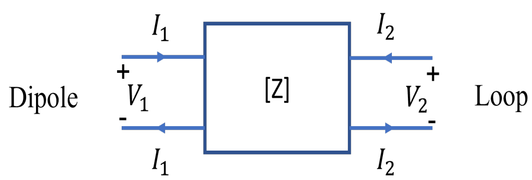

Fig. 2. The two-port network system.

The cocentered but nonorthogonal dipole and loop form a two-port network system as shown in Fig. 2. The voltages at port 1 (i.e., at the dipole) and port 2 (i.e., at the loop) are [49]

$$\left.\begin{aligned} V_1 &= Z_{1,1}I_1 + Z_{1,2}I_2 \\ V_2 &= Z_{2,1}I_1 + Z_{2,2}I_2. \end{aligned}\right\} \tag{1}$$

When I_1 is set to zero in (1), $Z_{1,2}$ is expressed as

$$Z_{1,2} = \left.\frac{V_1}{I_2}\right|_{I_1=0}.$$

$Z_{1,2}$ is the mutual impedance measured at the dipole when it is open-circuited and loop is excited. When I_2 is set to zero, $Z_{2,1}$ is expressed as

$$Z_{2,1} = \left.\frac{V_2}{I_1}\right|_{I_2=0}.$$

$Z_{2,1}$ is the mutual impedance measured at the loop when it is open-circuited and the dipole is excited. $Z_{1,1} = \frac{V_1}{I_1}$ and $Z_{2,2} = \frac{V_2}{I_2}$ represent the self-impedances when $I_2 = 0$ and $I_1 = 0$, respectively.

IV. Method of Moments Simulation

The Method of Moments (MoM) [50] is a popular numerical solution to many electromagnetic field problems such as antenna radiation and impedance. One of the simulation software that implements the MoM is "EMCoS Antenna VLab" [51].

In this paper, VLab obtains the entries of the 2×2 mutual impedance matrix in (2) that vary with the four independent variables, namely, dipole length ($\frac{L}{\lambda}$), the loop circumference ($\frac{C}{\lambda} = \frac{2\pi R}{\lambda}$), the skew angle or orthogonality φ, and the rotational angle β.

$$\mathbf{Z} = \begin{bmatrix} Z_{1,1} & Z_{1,2} \\ Z_{2,1} & Z_{2,2} \end{bmatrix} \tag{2}$$

In all VLab simulations, both the dipole and the loop always have a core radius of $1 \times 10^{-5}\lambda$, the dipole always has a feeding gap of $\frac{\lambda}{50}$, whereas the loop always has a feeding gap of $\frac{1}{8}^{\circ}$. The range of values of the four independent variables are: (i) the skew angle between the two axes, $\varphi \in [1^{\circ}, 45^{\circ}]$, (ii) the dipole's azimuth rotational angle, $\beta \in [1^{\circ}, 90^{\circ}]$, (iii) the wavelength-normalized dipole length, $\frac{L}{\lambda} \in [0.10, 1.00]$, and (iii) the wavelength-normalized large loop circumference, $\frac{C}{\lambda} = \frac{2\pi R}{\lambda} \in [1, 4]$.

For every combination of the four independent variables $(\frac{C}{\lambda}, \frac{L}{\lambda}, \varphi, \beta)$, the mutual impedance matrix in (2) is obtained.

Due to the principle of reciprocity, $|Z_{1,2}| = |Z_{2,1}|$, which was also confirmed in the VLab simulation. The real-valued scalars to be modeled are the magnitude of the mutual impedance $|Z_{1,2}| = |Z_{2,1}|$, the magnitude of the dipole's self-impedance $|Z_{1,1}|$, the phase of the dipole's self-impedance $\angle Z_{1,1}$, the magnitude of the loop's self-impedance $|Z_{2,2}|$, and the phase of the loop's self-impedance $\angle Z_{2,2}$.

V. Model Fitting

The plots of $|Z_{1,2}| = |Z_{2,1}|$, $|Z_{1,1}|$, $\angle Z_{1,1}$, $|Z_{2,2}|$ and $\angle Z_{2,2}$ are carefully examined on all perspectives and then the candidate models are fitted.

Three major steps are followed to obtain the best fit model.

1) Form the objective function.
   The objective function in (3) describes the sum of squares error (SSE) between the the proposed model and the VLab data.

$$SSE = \sum \left(Z_{\textit{VLab}} - Z_{\textit{model}}\right)^2 \tag{3}$$

   The objective here is to minimize the SSE.
2) Find the optimized coefficients from the proposed model.
   The optimized coefficients $\{c_1, c_2, ..., c_q\}$ that minimize the SSE are obtained through (4).

$$\{c_1, c_2, ..., c_q\} = \arg\min_{c} \sum \left(Z_{\textit{VLab}} - Z_{\textit{model}}\right)^2 \tag{4}$$

   The ultimate goal here is to obtain the minimum number of coefficients or degrees-of-freedom.
3) Compute the R^2.
   The goodness-of-fit test is performed through the coefficient of determination or $R^2 \in [0, 1]$ in (5).

$$R^2 = 1 - \frac{SSE}{SST} \tag{5}$$

$$SST = \sum \left(Z_{\text{VLab}} - \bar{Z}_{\text{VLab}}\right)^2 \tag{6}$$

where SST in (6) denotes the sum of squares total and $\bar{Z}_{\text{VLab}}$ indicates the mean of observed VLab data. The ultimate goal is to select the best fit model as evidenced by the model's R^2 (i.e., the closer the value of R^2 to 1, the better) and the model with fewer degrees-of-freedom.

VI. Model of the Magnitude of Mutual Impedance $|Z_{1,2}| = |Z_{2,1}|$

The best fit model for the magnitude of the mutual impedance is

$$\begin{aligned} &|Z_{1,2}| = |Z_{2,1}| \\ \approx\ & \left|\left(a_1 + a_2 \cos\left(a_3 \frac{C}{\lambda} + a_4\right) \exp\left(-\frac{C}{\lambda} + a_5 \frac{L}{\lambda}\right)\right)\right| \\ & |\sin(\varphi)||\sin(a_6\beta)| \end{aligned} \tag{7}$$

where

$$\begin{aligned} a_1 &:= 19.1651 \\ a_2 &:= 77.1140 \\ a_3 &:= 0.9234\pi \\ a_4 &:= -1.3128\pi \\ a_5 &:= 4.8423 \\ a_6 &:= 0.3149\pi. \end{aligned}$$

The coefficient of determination or R^2 is 0.9866. This means that only 1.34% of the variation from the VLab data was not explained by the model in (7).

A more refined expression may be obtained when the optimized coefficient values are rounded off to $a_1 = 20, a_2 = 75, a_3 = \frac{23}{25}\pi, a_4 = -\frac{131}{100}\pi, a_5 = \frac{24}{5}, a_6 = \frac{\pi^2}{10}$, giving an R^2 of 0.9807.

The model of the magnitude of mutual coupling $|Z_{1,2}| = |Z_{2,1}|$ in (7) is dependent on the wavelength-normalized loop circumference $\frac{C}{\lambda}$, wavelength-normalized dipole length $\frac{L}{\lambda}$, the skew angle φ and the rotational angle β.

$|Z_{1,2}| = |Z_{2,1}|$ is proportional to $|\sin(\varphi)|$. Stronger mutual coupling exists when the skew angle $|\varphi|$ approaches 90° (i.e., the dipole and loop would become more parallel). Hence, $|Z_{1,2}| = |Z_{2,1}|$ monotonically increases as suggested by the non-negative factor $|\sin(\varphi)|$ in (7). This is due to the increasing magnitude of the induced current as the dipole tilts towards the horizontal loop. When $\varphi = 0$, $|Z_{1,2}| = |Z_{1,2}| = 0$ (i.e., no mutual coupling). Conforming with the existing electromagnetic principles, the multiplicative factor $|\sin(\varphi)|$ is due to the projection of electric field from the driving dipole on the induced loop when the dipole is skewed by an angle $|\varphi|$.

$|Z_{1,2}| = |Z_{2,1}|$ monotonically increases as β increases with the multiplicative factor $|\sin(a_6\beta)|$. As the dipole through the rotational angle β moves away from the feed-point, the dipole and loop's electromagnetic fields would become more aligned, hence intensifying the mutual coupling. At a special case where $\beta = 0$, $|Z_{1,2}| = |Z_{1,2}| = 0$ for all values of φ.

(7) can be broken down into (8) and (9) to further discuss the conformance of the results to existing electromagnetic principles. Fig. 3 plots the relationship described in (9) and clearly illustrates the behavior mentioned above due to the effects of varying skew angle φ and rotational angle β.

$$\frac{|Z_{1,2}|}{K\left(\frac{C}{\lambda}, \frac{L}{\lambda}\right)} = \frac{|Z_{2,1}|}{K\left(\frac{C}{\lambda}, \frac{L}{\lambda}\right)} \approx |\sin(\varphi)||\sin(c_6\beta)|, \tag{8}$$

$$\begin{aligned} |Z_{1,2}||\csc(\varphi)||\csc(a_6\beta)| &= |Z_{2,1}||\csc(\varphi)||\csc(a_6\beta)| \\ &\approx K\left(\frac{C}{\lambda}, \frac{L}{\lambda}\right), \end{aligned} \tag{9}$$

where

$$\begin{aligned} & K\left(\frac{C}{\lambda}, \frac{L}{\lambda}\right) \\ := & \left|a_1 + a_2 \cos\left(a_3 \frac{C}{\lambda} + a_4\right) \exp\left(-\frac{C}{\lambda} + a_5 \frac{L}{\lambda}\right)\right|. \end{aligned} \tag{10}$$

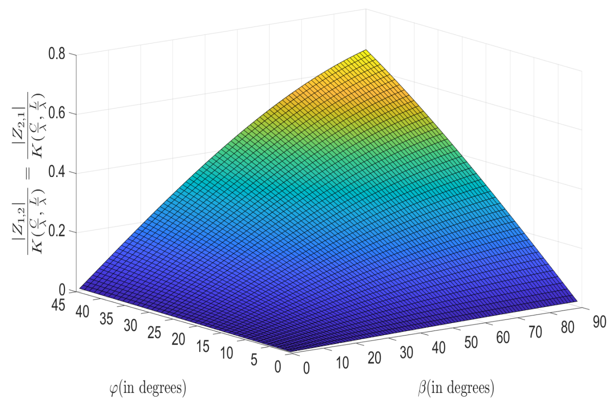

Fig. 3. How $|Z_{1,2}| = |Z_{2,1}|$ varies with the skew angle φ and rotational angle β.

$K\left(\frac{C}{\lambda}, \frac{L}{\lambda}\right)$ in (10) describes the effect of loop circumference and dipole length on $|Z_{1,2}| = |Z_{1,2}|$. This is shown in Fig. 4. The wavelength-normalized loop circumference $\frac{C}{\lambda}$ affects $|Z_{1,2}| = |Z_{1,2}|$ by causing an oscillation that exponentially decays with increasing loop circumference as shown in Figure 5. This is true in terms of electromagnetics since the current nonuniformity occurs for loop's $\frac{C}{\lambda} > 0.4\pi$ which produces a cosine distribution along the loop.

$|Z_{1,2}| = |Z_{1,2}|$ monotonically increases with the increasing wavelength-normalized dipole length $\frac{L}{\lambda}$(i.e., $\exp\left(a_5 \frac{L}{\lambda}\right)$). This conforms with the existing electromagnetic principles as the current carrying capacity of the dipole increases with its length, hence increasing the induced current and contributing to a higher magnitude of mutual impedance.

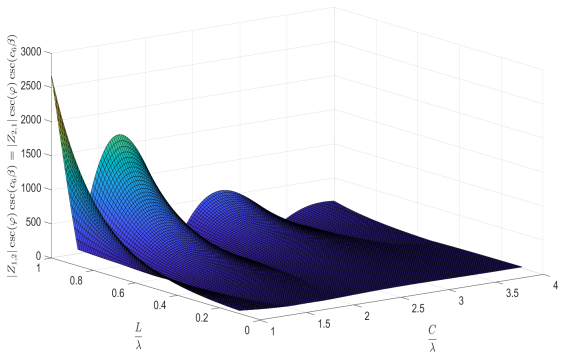

Fig. 4. How $|Z_{1,2}| = |Z_{2,1}|$ varies with the wavelength-normalized loop circumference $\frac{C}{\lambda}$ and wavelength-normalized dipole length $\frac{L}{\lambda}$.

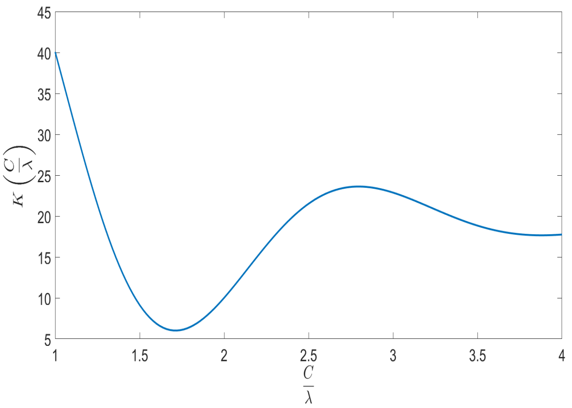

Fig. 5. How $K\left(\frac{C}{\lambda}\right)$ varies with $\frac{C}{\lambda}$.

VII. Model of the Magnitude of Dipole's Self-Impedance $|Z_{1,1}|$

The best fit model for the magnitude of $Z_{1,1}$ is

$$|Z_{1,1}| \approx |b_1 + b_2 \exp(\beta - b_3\varphi)| \left(\frac{L}{\lambda} - b_4\right)^2 \quad (11)$$

where

$$\begin{aligned} b_1 &:= 24466.8076 \\ b_2 &:= 31.4922 \\ b_3 &:= 2.9000 \\ b_4 &:= 0.4755. \end{aligned}$$

The model of $|Z_{1,1}|$ in (11) obtained an R^2 of 0.9759. This means that only 2.41% of the variation from the VLab data was not explained by the model.

A more refined expression may be obtained when the optimized coefficient values are rounded off to $b_1 = 25000, b_2 = 30, b_3 = \frac{29}{10}, b_4 = \frac{951}{2000}$, giving an R^2 of 0.9752.

As seen from the model in (11), the excited dipole's self-impedance $|Z_{1,1}|$ is dependent on the wavelength-normalized dipole length $\frac{L}{\lambda}$, the skew angle φ and the rotational angle β but independent of the wavelength-normalized loop circumference $\frac{C}{\lambda}$.

Rewriting (11) in the form of (12), we can observe that $|Z_{1,1}|$ is affected by φ and β only through the multiplicative factor $\psi(\varphi, \beta)$.

$$|Z_{1,1}| \approx \psi(\beta, \varphi)\, T\left(\frac{L}{\lambda}\right), \quad (12)$$

where

$$\psi(\beta, \varphi) := |b_1 + b_2 \exp(\beta - b_3\varphi)| \quad (13)$$

$$T\left(\frac{L}{\lambda}\right) := \left(\frac{L}{\lambda} - b_4\right)^2. \quad (14)$$

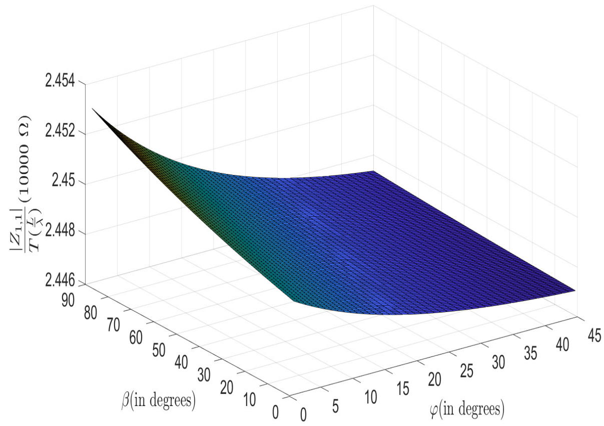

Fig. 6. How φ and β affect the magnitude of the dipole's self-impedance.

When the dipole skew away from orthogonality, $|Z_{1,1}|$ decreases and it exponentially increases with increasing rotational angle β. Fig. 6 illustrates these observations.

When the loop and dipole are orthogonal (i.e., $\varphi = 0, \beta = 0$), the model in (11) would degenerate to $|Z_{1,1}| \approx (b_1 + b_2)T\left(\frac{L}{\lambda}\right)$, which means that the dipole is fully isolated from the loop due to the absence of mutual coupling.

A minimum value of $|Z_{1,1}|$ in (11) is obtained at $\frac{L}{\lambda} = 0.4755$. The parabolic expression described in (14) and shown in Fig. 7 conforms to the dipole's input impedance characteristics where the first resonance and anti-resonance appear near $\frac{L}{\lambda} = 0.5$ and $\frac{L}{\lambda} = 1.0$, respectively.

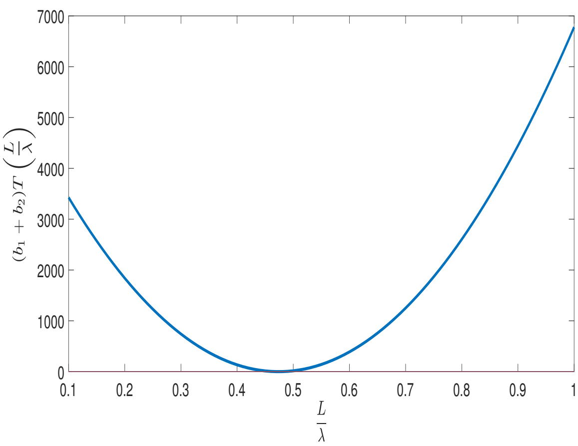

Fig. 7. How $\frac{L}{\lambda}$ affects the magnitude of isolated dipole's self-impedance.

From the theory in antenna array, the sum of mutual impedance and self-impedance is equal to the input impedance. Moreover, when the mutual impedance is zero (i.e., the dipole is fully isolated from the loop), the dipole's input impedance is equal to its self-impedance.

VIII. Model of the Dipole's Self-Impedance Phase $\angle Z_{1,1}$

The best fit model for the phase of $Z_{1,1}$ is

$$\angle Z_{1,1} \approx (c_1 + c_2 \exp(-c_3\beta + c_4\varphi)) \cos\left(c_5 \frac{L}{\lambda} + c_6\right) \tag{15}$$

where

$$\begin{aligned} c_1 &:= 1.6731 \\ c_2 &:= 0.0015 \\ c_3 &:= 4.0815 \\ c_4 &:= 3.2711 \\ c_5 &:= 1.9863\pi \\ c_6 &:= 2.5569\pi. \end{aligned}$$

The model of $\angle Z_{1,1}$ in (15) obtained an R^2 value of 0.8878. This means that only 11.22% of the variation from the VLab data was not explained by the model.

A more refined expression may be obtained when the optimized coefficient values are rounded off to $c_1 = \frac{17}{10}, c_2 = \frac{3}{2000}, c_3 = 4, c_4 = \frac{13}{4}, c_5 = 2\pi, c_6 = \frac{51}{20}\pi$, giving an R^2 of 0.8874.

$\angle Z_{1,1}$ is independent of the wavelength-normalized loop circumference $\frac{C}{\lambda}$ but dependent on the wavelength-normalized dipole length $\frac{L}{\lambda}$, the skew angle φ and the rotational angle β.

(15) can be broken down into two multiplicative factors $M(\beta, \varphi)$ and $\cos\left(c_5 \frac{L}{\lambda} + c_6\right)$ as shown in (16).

$$\angle Z_{1,1} \approx M(\beta, \varphi) \cos\left(c_5 \frac{L}{\lambda} + c_6\right), \tag{16}$$

where

$$M(\beta, \varphi) := c_1 + c_2 \exp(-c_3\beta + c_4\varphi). \tag{17}$$

In the multiplicative factor $M(\beta, \varphi)$ in (17), $\angle Z_{1,1}$ increases exponentially as the skew angle $|\varphi|$ approaches 90°, while it decreases as the rotational angle $|\beta|$ approaches 90°. This is illustrated in Fig. 8.

$\angle Z_{1,1}$ register negative and positive values due to the muliplicative factor $\cos\left(c_5 \frac{L}{\lambda} + c_6\right)$. In fact, with $\frac{L}{\lambda} \in [0.1, 0.47]$ and $\frac{L}{\lambda} \in [0.98, 1.0]$, negative $\angle Z_{1,1}$ can be observed. Whereas, with $\frac{L}{\lambda} \in [0.48, 0.97]$, positive phase can be noticed. The points of zero crossings, i.e., near $\frac{L}{\lambda} = 0.50$ and near $\frac{L}{\lambda} = 1.0$ in Fig. 9 correspond with the dipole's resonant and anti-resonant lengths, respectively.

IX. Model of the Magnitude of Loop's Self-Impedance $|Z_{2,2}|$

The best fit model for the magnitude of $Z_{2,2}$ is

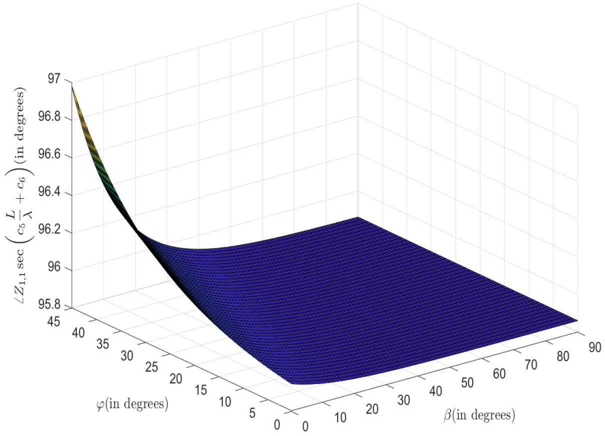

Fig. 8. How β and φ affect the phase of isolated dipole's self-impedance.

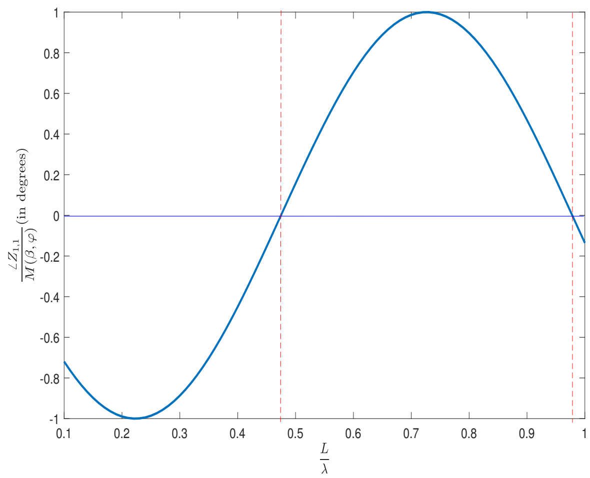

Fig. 9. How $\frac{L}{\lambda}$ affects the phase of isolated dipole's self-impedance.

$$\begin{aligned} |Z_{2,2}| \approx\ & d_1 \exp\left(-\left(\frac{\frac{C}{\lambda} - d_2}{d_3}\right)^2\right) \\ & + d_4 \exp\left(-\left(\frac{\frac{C}{\lambda} - d_5}{d_6}\right)^2\right) \\ & + d_7 \exp\left(-\left(\frac{\frac{C}{\lambda} - d_8}{d_9}\right)^2\right) \end{aligned} \tag{18}$$

where

$$\begin{aligned} d_1 &:= 6993 \\ d_2 &:= 1.499 \\ d_3 &:= 0.1252 \\ d_4 &:= 4874 \\ d_5 &:= 2.503 \\ d_6 &:= 0.1786 \\ d_7 &:= 4189 \\ d_8 &:= 3.507 \\ d_9 &:= 0.2032. \end{aligned}$$

The computed R^2 is 0.9102. This means that only 8.98% of the variability was not explained by the model.

A more refined expression may be obtained when the optimized coefficient values are rounded off to $c_1 = 7000, c_2 = \frac{3}{2}, c_3 = \frac{3}{25}, c_4 = 5000, c_5 = \frac{5}{2}, c_6 = \frac{3}{20}, c_7 = 4000, c_8 = \frac{7}{2}, c_9 = \frac{1}{5}$, giving an R^2 of 0.9013.

The excited loop's self-impedance $|Z_{2,2}|$ is dependent only on the wavelength-normalized loop circumference $\frac{C}{\lambda}$. The model in (18) follows a three-term Gaussian function. The three peaks on the curves are centered at approximately $c_2 = 1.50$, $c_5 = 2.50$, and $c_8 = 3.50$. This conforms with the theory of electromagnetics since the maximum directivity of the loop occurs near $\frac{C}{\lambda} = 1.50$, where the impedance is too large. The amplitude of the peaks, as shown in Fig. 10, decreases as $\frac{C}{\lambda}$ gets larger. From the theory on large loop antenna, the resonance (i.e., the magnitude of the impedance is minimum) occurs near $\frac{C}{\lambda} = 1.00$ and it is just repetitive near $\frac{C}{\lambda} = 2.00, 3.00$, and 4.00.

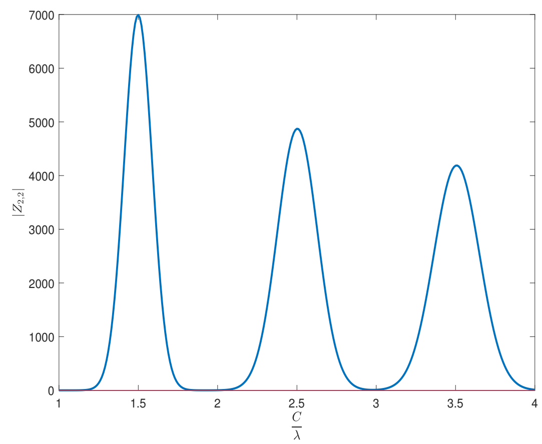

Fig. 10. How $\frac{C}{\lambda}$ affects the magnitude of loop's self-impedance.

X. Model of the Loop's Self-Impedance Phase $\angle Z_{2,2}$

The best fit model for the phase of $Z_{2,2}$ is

$$\angle Z_{2,2} \approx e_1 + e_2 \sin\left(e_3 \frac{C}{\lambda} + e_4\right) \exp\left(-e_5 \frac{C}{\lambda}\right) \tag{19}$$

where

$$\begin{aligned} e_1 &:= -10.6100 \\ e_2 &:= 99.7700 \\ e_3 &:= -1.9904\pi \\ e_4 &:= 3.0112\pi \\ e_5 &:= 0.09388. \end{aligned}$$

The model of $\angle Z_{2,2}$ in (19) obtained an R^2 of 0.9651. This means that only 3.49% of the variation from the VLab data was not explained by the model.

A more refined expression may be obtained when the optimized coefficient values are rounded off to $e_1 = -\frac{53}{5}, e_2 = 100, e_3 = -\frac{199}{100}\pi, e_4 = \frac{301}{100}\pi, e_5 = \frac{19}{200}$, giving an R^2 of 0.9651.

The model in (19) resembles an expression of a damped sinewave or an exponential damping, where the peak-to-peak amplitudes of $\angle Z_{2,2}$ decrease with each oscillation and with increasing $\frac{C}{\lambda}$. The positive peaks appear near $\frac{C}{\lambda} = 1.25, 2.25, 3.25$, while the negative peaks appear near $\frac{C}{\lambda} = 1.75, 2.75, 3.75$, as illustrated in Fig. 11. The zero crossings that occur near $\frac{C}{\lambda} = 1.5, 2.5, 3.5$ coincide with the peaks of $|Z_{2,2}|$ as shown Fig.10.

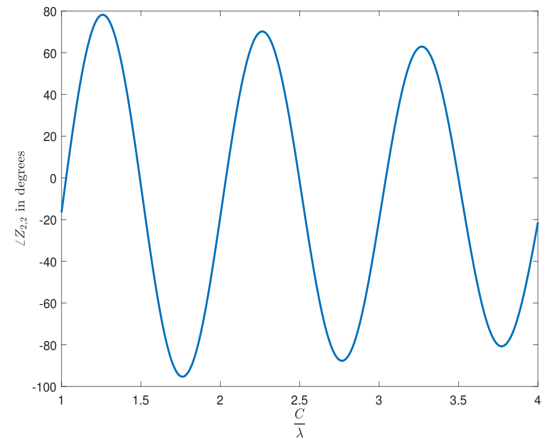

Fig. 11. How $\frac{C}{\lambda}$ affects the phase of loop's self-impedance.

Due to the loop's resonance near $\frac{C}{\lambda} = 1.00, 2.00, 3.00$, and 4.00, the phase of the loop is zero because there is no reactance.

XI. Conclusion

This paper successfully obtained low-dimensional models of the magnitude of mutual impedance and the magnitude and phase of the dipole and loop self-impedances for the cocentered but nonorthogonally oriented loop and dipole as evidenced by the high R^2 values, hence obtaining small fitting errors. The orthogonality of the COLD antenna pair may not be maintained in practical situations, thus the characterization of cocentered but nonorthogonally oriented loop and dipole is deemed important. The open literature presents complicated equations that involve complex integrals and nested summations for solving the mutual impedance and self-impedances of the loop and dipole. With the aid of EMCoS Antenna VLab, the obtained models provide very simple closed form expressions that are intuitive and conform with the existing electromagnetic principles.

References

[1] N. Kato, "Composite Antenna," U.S. Patent 8179329B2, May 15, 2012.

[2] X. -T. Wu, W. -J. Lu, J. Xu, K. F. Tong and H. -B. Zhu, "Loop-Monopole Composite Antenna for Dual-Band Wireless Communications," *IEEE Antennas and Wireless Propagation Letters*, vol. 14, pp. 293-296, October 2015.

[3] G. Liu, W. Lu and H. Zhu, "A novel loop-dipole composite unidirectional antenna for broadband wireless communications," *IEEE International Symposium on Microwave, Antenna*, Propagation and EMC Technologies for Wireless Communications, pp. 295-299, 2013.

[4] W. Lu, G. Liu, K. F. Tong and H. Zhu, "Dual-Band Loop-Dipole Composite Unidirectional Antenna for Broadband Wireless Communications," *IEEE Transactions on Antennas and Propagation*, vol. 62, no. 5, pp. 2860-2866, May 2014.

[5] S. Ahdi Rezaeieh, K. S. Bialkowski, A. Zamani and A. M. Abbosh, "Loop-Dipole Composite Antenna for Wideband Microwave-Based Medical Diagnostic Systems With Verification on Pulmonary Edema Detection," *IEEE Antennas and Wireless Propagation Letters*, vol. 15, pp. 838-841, December 2016.

[6] W. -J. Lu, W. -H. Zhang, K. F. Tong and H. -B. Zhu, "Planar Wideband Loop-Dipole Composite Antenna," *IEEE Transactions on Antennas and Propagation*, vol. 62, no. 4, pp. 2275-2279, April 2014.

[7] S. Ebihara, K. Matsubara, and N. Nagao. "Cocentered Orthogonal Loop and Dipole Antenna for Borehole Radar." *International Conference on Ground Penetrating Radar*, pp.19-22, 2006.

[8] J. Li, P. Stoica & D. Zheng, "Efficient direction and polarization estimation with a COLD array," *IEEE Transactions on Antennas and Propagation*, vol. 44, no. 4, pp. 539-547 April 1996.

[9] J. Li & D. Zheng, "Parameter estimation using RELAX with a COLD array," *Circuits, Systems, and Signal Processing*, vol. 17, no. 4, pp. 471-481, July 1998.

[10] J.-C. Huang, Y.-W. Shi & J.-W. Tao, "Closed-form estimation of DOA and polarization for multisource with a uniform circular array," *International Conference on Machine Learning and Cybernetics*, vol. 7, pp. 4469-4474, 2005.

[11] C.-H. Lin, W.-H. Fang, W.-S. Yang & J.-D. Lin, "SPS-ESPRIT for joint DOA and polarization estimation with a COLD array," *IEEE Antennas and Propagation Society International Symposium*, pp. 1136-1139, 2007.

[12] J. Tao, H. Xu & J.-W. Tao, "Closed-form direction finding for multiple sources based on uniform circular arrays with trimmed vector sensor," *World Congress on Intelligent Control and Automation*, pp. 2392-2395, 2008.

[13] R. Boyer, "Analysis of the COLD uniform linear array," *IEEE Workshop on Signal Processing Advances in Wireless Communications*, pp. 563-567, 2009.

[14] L. Liang, T. Jian-wu & C. Wei, "DOA estimation based on sparse and nonuniform COLD array," *International Conference on Communications and Mobile Computing*, vol. 1, pp. 391-395, 2009.

[15] T. Jun, T. Yantao, C. Wei & Y. Mao, "DOA estimation algorithm of scattered sources based on polarization sensitive sensor array," *Chinese Journal of Scientific Instrument*, vol. 31, no. 6, pp. 1224-1233, June 2010.

[16] M. N. El Korso, R. Boyer, A. Renaux & S. Marcos, "Statistical resolution limit of the uniform linear cocentered orthogonal loop and dipole array," *IEEE Transactions on Signal Processing*, vol. 59, no. 1, pp. 425-431, January 2011.

[17] D. T. Vu, A. Renaux, R. Boyer & S. Marcos, "Weiss-Weinstein bound and SNR threshold analysis for DOA estimation with a COLD array," *IEEE Statistical Signal Processing Workshop*, pp. 13-16, 2011.

[18] Y. Wang & Y. Wu, "Direction and polarization estimation using quaternion and polarization rotation matrix," *IEEE Symposium on Electrical & Electronics Engineering*, pp. 319-322, 2012.

[19] L. Wang, G. Wang & Z. Chen, "Joint DOA-polarization estimation based on uniform concentric circular array," *Journal of Electromagnetic Waves and Propagation*, vol. 27, no. 13, pp. 1702-1714, 2013.

[20] Z. Liu & T. Xu, "Source localization using a non-cocentered orthogonal loop and dipole (NCOLD) array," *Chinese Journal of Aeronautics*, vol. 26, no. 6, pp. 1471-1476, 2013.

[21] Y. Xu, J. Ma & Z. Liu, "Polarization sensitive PARAFAC beamforming for near-field/far-field signals using co-centered orthogonal loop and dipole pairs," *IEEE China Summit and International Conference on Signal and Information Processing* , pp. 616-620, 2013.

[22] L. Wang, L. Yang, G. Wang, S. Wang, "DOA and Polarization Estimation Based on Sparse COLD Array," *Wireless Personal Communications*, vol. 85, no. 4, pp.2447-2462, December 2015.

[23] Y. Tian & H. Xu, "DOA, power and polarization angle estimation using sparse signal reconstruction with a COLD array," *International Journal of Electronics and Communications*, vol. 69, no. 11, pp. 1606-1612, July 2015.

[24] H. Chen, W. Wang and W. Liu, "Joint DOA, Range, and Polarization Estimation for Rectilinear Sources With a COLD Array," *IEEE Wireless Communications Letters*, vol. 8, no. 5, pp. 1398-1401, October 2019.

[25] W. Si, Y. Wang and C. Zhang, "2D-DOA and Polarization Estimation Using a Novel Sparse Representation of Covariance Matrix With COLD Array," *IEEE Access*, vol. 6, pp. 66385-66395, 2018

[26] T. Bao, A. Breloy, M. N. El Korso, K. Abed-Meraim and H. H. Ouslimani, "Performance analysis of direction-of-arrival and polarization estimation using a non-uniform linear COLD array," *Seminar on Detection Systems Architectures and Technologies*, pp. 1-5, 2017.

[27] T. Bao and D. Zhou, "Cramér-Rao Bounds for Non-Uniform Linear Cocentered Orthogonal Loop and Dipole Array," *International Applied Computational Electromagnetics Society Symposium*, pp. 1-2, 2018.

[28] A. M. Elbir, "A Novel Data Transformation Approach for DOA Estimation With 3D Antenna Arrays in the Presence of Mutual Coupling," *IEEE Antennas and Wireless Propagation Letters*, vol. 16, pp. 2118-2121, April 2017.

[29] Z. Zheng, C. Yang, W. -Q. Wang and H. C. So, "Robust DOA Estimation Against Mutual Coupling With Nested Array," *IEEE Signal Processing Letters*, vol. 27, pp. 1360-1364, July 2020.

[30] Z. Ye and C. Liu, "2D DOA Estimation in the Presence of Mutual Coupling," *IEEE Transactions on Antennas and Propagation*, vol. 56, no. 10, pp. 3150-3158, October 2008.

[31] T. T. Zhang, Y. L. Lu and H. T. Hui, "Compensation for the mutual coupling effect in uniform circular arrays for 2D DOA estimations employing the maximum likelihood technique," *IEEE Transactions on Aerospace and Electronic Systems*, vol. 44, no. 3, pp. 1215-1221, July 2008.

[32] Y. I. Wu, G. P. Arada, W. -Y. Tam and K. T. Wong, "Mis-modeling and mis-correction of mutual coupling in an antenna array — A case study in the context of direction finding using a linear array of identical dipoles," *IEEE International Conference on Signal and Image Processing*, pp. 447-451, 2016.

[33] Y. I. Wu, G. P. Arada, K. T. Wong and W. Tam, "Electromagnetic coupling matrix modeling and ESPRIT-based direction finding — A case study using a uniform linear array of identical dipoles," *IET International Conference on Intelligent Signal Processing*, pp. 1-5, 2015.

[34] G. P. Arada, "How Varying the Dipole Lengths of a Uniform Linear Array Affects the Performance of an ESPRIT based Direction Finding Algorithm," *International Journal of Circuits, Systems and Signal Processing*, vol. 14, pp. 952-956, 2020.

[35] Y. Yu, H. Lui, C. H. Niow and H. T. Hui, "Improved DOA Estimations Using the Receiving Mutual Impedances for Mutual Coupling Compensation: An Experimental Study," *IEEE Transactions on Wireless Communications*, vol. 10, no. 7, pp. 2228-2233, July 2011.

[36] J. Xie, L. Wang and J. Su, "Efficient DOA Estimation Algorithm for Noncircular Sources Under Unknown Mutual Coupling," *IEEE Sensors Letters*, vol. 2, no. 3, pp. 1-4, September 2018.

[37] W. Yujiang and N. Zaiping, "On the improvement of the mutual coupling compensation in DOA estimation," *Journal of Systems Engineering and Electronics*, vol. 19, no. 1, pp. 1-6, Feb. 2008.

[38] J. S. Belrose and S. White, "On validation of NEC-MoM: a useful tool for MF antenna system design," *IEEE Antennas and Propagation Society Symposium*, vol.3 pp. 2891-2894, 2004.

[39] Y. Zhang, T. K. Sarkar, H. Moon, M. Taylor, D. G. Donoro and M. Salazar-Palma, "Parallel MoM simulation of complex EM problems," *IEEE Antennas and Propagation Society International Symposium*, pp. 1-4, 2009.

[40] K. Alkhalifeh, G. Hislop, N. A. Ozdemir and C. Craeye, "Efficient MoM Simulation of 3D Antennas in the Vicinity of the Ground," textslIEEE Transactions on Antennas and Propagation, vol. 64, no. 12, pp. 5335- 5344, December 2016.

[41] J. W. R. Cox, "Corroboration of a moment-method calculation of the maximum mutual coupling between two HF antennas mounted on a helicopter," *IEE Proceedings H - Microwaves, Antennas and Propagation*, vol. 140, no. 2, pp. 113-120, 1993.

[42] G. P. Arada and T. Hirano, "The Effects of Varying the Location of Antenna Feed Gaps on Mutual Coupling Between Orthogonal Circular Loops," *International Conference on Electronics, Information, and Communication*, pp. 1-6, 2020.

[43] G. P. Arada, Y. I. Wu, K. T. Wong, W.-Y. Tam, S. Khan and C. J. Fulton, "How Two Crossed Dipoles' Impedance Varies With Their Non-Orthogonality, Length & Separation," *Radio Science*, vol. 57, no. 4, pp. 1-12, April 2022.

[44] S. Shastri, K. Shah & R. Shekhar, "Modified circular polarized loop antenna," *IEEE International Conference on Recent Advances in Microwave Theory & Applications*, pp. 934-936, 2008.

[45] B. Li & Q. Xue, "Polarization-reconfigurable omnidirectional antenna combining dipole and loop radiators," *IEEE Antennas and Wireless Propagation Letters*, vol. 12, pp. 1102-1105, 2013.

[46] F. Tefiku & C. A. Grimes, "Coupling between elements of electrically small compound antennas," *Microwave and Optical Technology Letters*, vol. 22, no. 1, pp. 16-21, July 1999.

[47] R. C. Hansen, "The electrically small dipole-loop," *The Applied Computational Electromagnetics Society Journal*, vol. 16, no. 3, pp. 228-231, November 2001.

[48] S. R. Best, "The electrically small dipole-loop pair revisited," *IEEE Antennas and Propagation Society International Symposium*, pp. 2265-2268, 2007.

[49] C. A. Balanis, *Antenna Theory: Analysis and Design*, Hoboken, New Jersey, USA: Wiley, 1997.

[50] R. F. Harrington, *Field Computation by Method of Moments*, Macmillan, 1968.

[51] EMCoS Consulting and Software, *Tri-D User's Manual*, Georgia, USA: EMCoS, 2009.

Gerald P. Arada obtained a B.S. in 1997 from the Polytechnic University of the Philippines (Metro Manila, Philippines), and an M.Eng. in 2006 from De La Salle University (Metro Manila, Philippines) – both in Electronics and Communications Engineering. He received a Ph.D. from the Hong Kong Polytechnic University in 2018. G. P. Arada was an Instructor at the Polytechnic University of the Philippines between 1997 and 2006, then an engineer with Analog Devices, Inc. (Cavite, Philippines) during 2006-2009. Since 2009, he has been a faculty of De La Salle University, now as an Associate Professor. His research interests are in antennas, array signal processing and wireless communications.